Thermoelectric Effect across the Metal−Insulator Domain Walls in VO₂ Microbeams

J. Cao,[†,‡,⊥] W. Fan,[†,§,⊥] H. Zheng,[‡,‖] and J. Wu*[,†,‡]

Department of Materials Science and Engineering, University of California, Berkeley, Berkeley, California 94720, Materials Sciences Division, National Center for Electron Microscopy, Lawrence Berkeley National Laboratory, Berkeley, California 94720, and Department of Thermal Science and Energy Engineering, University of Science and Technology of China, Hefei, China

ABSTRACT

We report on measurements of Seebeck effect in single-crystal VO₂ microbeams across their metal−insulator phase transition. One-dimensionally aligned metal−insulator domain walls were reversibly created and eliminated along single VO₂ beams by varying temperature, which allows for accurate extraction of the net contribution to the Seebeck effect from these domain walls. We observed significantly lower Seebeck coefficient in the metal−insulator coexisting regime than predicted by a linear combination of contributions from the insulator and metal domains. This indicates that the net contribution of the domain walls has an opposite sign from that of the insulator and metal phases separately. Possible origins that may be responsible for this unexpected effect were discussed in the context of complications in this correlated electron material.

High-performance thermoelectric materials are currently one of the focuses in materials research for energy conversion technologies.[1−4] A good thermoelectric material should have a relatively high thermopower (Seebeck coefficient).[1,5] Quest for an ever higher Seebeck coefficient has led to material innovations where the electron density of state is engineered by homogeneous doping of single-phase materials.[4] Alternatively, interfacing different materials has been proposed as a means to enhance the Seebeck effect from that of the constituent materials alone. For example, in addition to the conventional bulk Seebeck effect, extra thermal transport is expected by thermionic emission of free carriers over an energy barrier that is formed in the Schottky junction between a metal and a semiconductor, or from the band offset between two different semiconductors.[6−8] This effect would enhance the thermoelectric performance of the structure beyond that of each single-phase material alone. Indeed, such an enhancement of the overall Seebeck coefficient has been observed in InGaAs/InGaAlAs superlattices embedded with randomly distributed ErAs nanoparticles.[9] Recently, Seebeck coefficient was also reported to be enhanced by a single tunneling junction in individual Au nanowires.[10] Effect of single or a few Schottky junctions on the Seebeck coefficient has not been experimentally tested, mainly due to the lack of materials suitable for accurate determination of the small change in the Seebeck coefficient. We explore this effect using a special material system, VO₂ microbeams, where one or a few Schottky junctions can be reversibly created and eliminated in the plane perpendicular to the current and heat flow direction. This offers a material platform where the thermoelectric effect can be measured from the same specimen with or without the Schottky junction, so that an accurate extraction of the net junction effect becomes possible.

VO₂ undergoes a first-order metal−insulator Mott transition (MIT) at 68 °C from a high-temperature metallic (M) phase to a low-temperature insulating (I) phase. This electronic transition is accompanied by a structural phase transition from a high-temperature tetragonal structure to a low-temperature monoclinic structure,[11] causing the specimen to spontaneously shrink by 1% along the tetragonal *c*-axis.[11−13] As expected from the lattice constant change, a uniaxial compressive (tensile) stress along the *c*-axis direction would drive the system toward the M (I) phase. It has been observed that when a *c*-axis orientated VO₂ beam is clamped on a SiO₂ surface, uniaxial strain is accumulated in the VO₂ as a result of elastic mismatch across the interface, which

* To whom correspondence should be addressed. E-mail: wuj@berkeley.edu.
† University of California, Berkeley.
‡ Materials Sciences Division, Lawrence Berkeley National Laboratory.
§ University of Science and Technology of China.
‖ National Center for Electron Microscopy, Lawrence Berkeley National Laboratory.
⊥ These authors contributed equally to this work.

subsequently organizes multiple M−I domains one dimensionally along the VO_2 beam near 68 °C.[14] The M−I domain wall is the epitaxial interface between the monoclinic and tetragonal structures with an interfacial energy density of about 25 mJ/m.[2] It is believed that the MIT occurs as a result of a symmetric splitting of the t_{2g} band formed mainly by the vanadium 3d states.[11] A bandgap of ∼0.6 eV is opened near the Fermi level within this band, which aligns the M-phase Fermi level inside the bandgap of the I-phase VO_2. A metal−semiconductor Schottky junction therefore forms at the M−I domain wall with a junction height of ∼0.3 eV and width of ∼15 nm (see Supporting Information). This provides a convenient system to probe the junction effect in thermoelectrics. Interesting electron filtering effects have been proposed and observed across this self-developed Schottky junction in VO_2.[15,16] Thermoelectric effect across the junction has not been directly measured. The reversible generation and elimination of such a junction within a chemically homogeneous material system allow for accurate determination of the junction effect. An M domain emerging in I phase will create two M−I Schottky junctions with one forward biased and the other reverse biased electrically. A Peltier cooling will occur at the reversely biased junction and a Peltier heating at the forward biased junction. Additional heat flow is thus carried by the drift current due to the existence of the junctions. In this letter, we report on direct measurements of the domain wall effect on the Seebeck voltage in thermally biased VO_2 microbeams.

We synthesized single-crystal VO_2 nano- and microbeams on quartz surface using the vapor transport method developed by the Park group.[17] These beams have rectangular cross section and grow along the tetragonal c-axis direction with width 50 nm to 2 μm and length up to 100 μm. Most of these beams were grown with bottom side firmly clamped on the quartz surface due to the high growth temperature (∼980 °C). Under white light illumination, VO_2 exhibits sharp optical contrast between the M (dark reflection) and I (bright reflection) phases.[14] This is illustrated in Figure 1a, where M−I domains were seen in a range of temperatures near 68 °C. The domains were one-dimensionally organized along the VO_2 microbeam with each domain spanning the entire beam width. This domain configuration was formed to maximally relax the strain energy in the system.[14] Figure 1b shows a high-resolution transmission electron microscopy image of a VO_2 nanobeam, where the coexistence of M and I phases is clearly seen. Such a phase coexistence in this nanobeam was probably caused by large surface strain which was shown to be able to stabilize the M phase even at room temperature.[18] The two phases in Figure 1b were indexed to monoclinic (I) and tetragonal (M) structures with a (010) plane in the former jointed with the ($\bar{2}$00) plane in the latter as the domain wall. It is seen from Figure 1b that the domain wall is epitaxial without dislocation, as expected, and spans over several lattice spacing in thickness.

Devices for Seebeck measurements were fabricated using these VO_2 beams. Figure 2a shows a scanning electron microscopy image of a typical device. The four metal contacts and heaters were patterned on a single as-grown
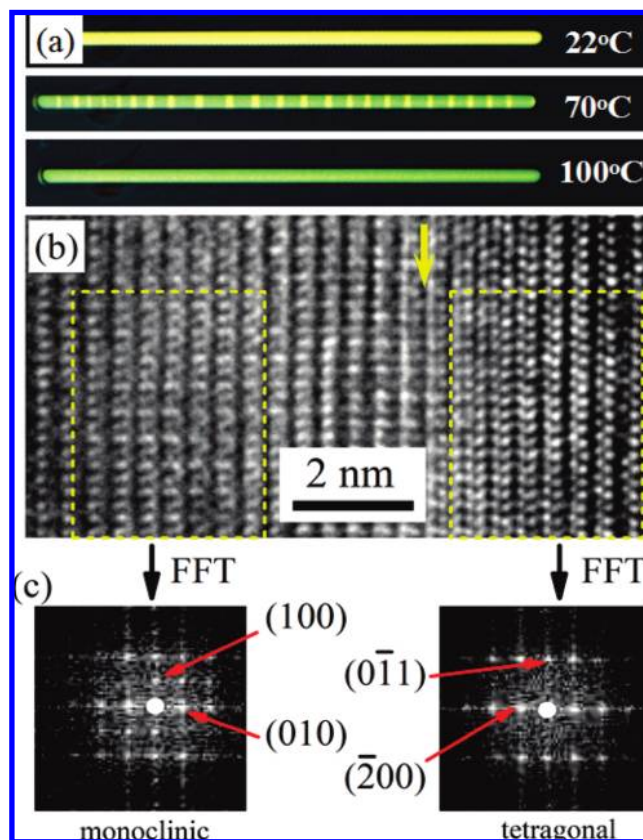

Figure 1. (a) Optical images of a VO_2 microbeam (2 μm width) bottom clamped on a quartz surface showing one-dimensional organization of M (dark)/I (bright) domains near the natural MIT temperature. (b) High-resolution TEM image of a VO_2 nanobeam showing coexisting M and I phases and the domain wall between them across a few lattice planes. The yellow arrow denotes where the vertical domain wall centers, as determined from selected-area FFT in (c). (c) Fast-Fourier transform (FFT) of selected areas in (b), showing the monoclinic indexing (along [00$\bar{1}$] zone axis) and tetragonal indexing (along [011] zone axis), respectively.

VO_2 beam using standard photolithography and sputtered with 20 nm Ti and 400 nm Au, which is known to form Ohmic contact on VO_2.[14] The VO_2 resistance was measured through these electrodes in a four-probe geometry. The heater was patterned next to and perpendicular to the VO_2 beam to generate a temperature gradient across the beam length direction.[3,19] The firm bottom clamping of the as-grown beams ensured good thermal contact with the quartz substrate, such that the temperature gradient in the beam was constant, independent of the M−I domain configuration in the beam, and dictated by the temperature distribution in the substrate. Each contact electrode was branched out with four metal leads, so that the change in the electrode resistance could be accurately measured as a function of temperature and calibrated to serve as a local temperature sensor on the VO_2 beam at the contact point. The electrodes have much higher thermal conductivity than the substrate and VO_2. Therefore the VO_2 beam underneath the electrodes has a relatively constant temperature profile than the exposed part. Finite-element modeling was performed using COMSOL Multiphysics to verify the measured temperature drop between electrodes. A DC current was flowing in the
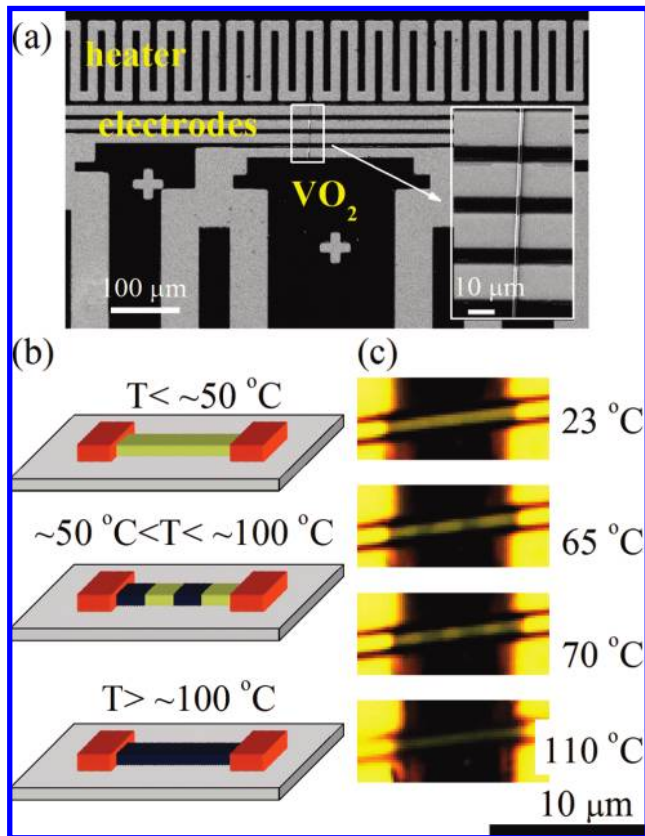
Figure 2. (a) SEM image of a VO$_2$ device used for Seebeck measurements showing the local heater, the electrodes, and the VO$_2$ beam. A global heater is glued to the back of the device chip. (b) Schematics of multiple M−I domains forming along the device at intermediate temperatures. (c) Optical images of a typical VO$_2$ device taken at global temperature equal to 23, 65, 70, and 110 °C, showing pure I and M phases at low and high temperatures, respectively, and coexistence of a few I and M domains at intermediate temperatures.

patterned heater to create a temperature difference between electrodes, and the Seebeck coefficient of the VO$_2$ beam was determined by measuring the thermoelectric voltage drop between the hot and cold electrodes

$$S(T_{global}) = -(V_{hot} - V_{cold})/(T_{hot} - T_{cold}) \qquad (1)$$

Here T_{global} is the global temperature of the device, which was controlled with a Lakeshore temperature controller equipped with a macroscopic resistive heater glued to the back side of the device chip and a small thermal couple glued close to the device on the chip surface.

As shown in Figure 2c and schematically in Figure 2b, the VO$_2$ beam is in pure I phase at low temperatures (<∼50 °C), and pure M phase at high temperatures (>∼100 °C). At intermediate temperatures (50−100 °C), M and I phases coexist. The domain pattern evolves as a function of temperature in consistence with previous reports.[14,20] The total resistance (R_{total}) of the middle segment of the VO$_2$ beam was measured as a function of T_{global} in a four-probe geometry. A typical R_{total} versus T_{global} curve is shown in Figure 3a. The curve shows steps that correspond to new M
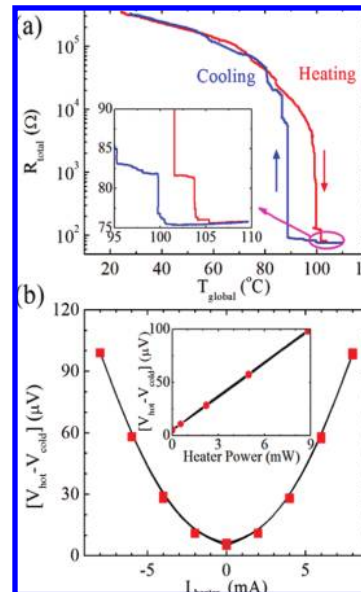

Figure 3. (a) Resistance of a VO$_2$ beam measured in four-probe geometry as a function of temperature at a ramping rate of 4 °C/min. Inset: a close-up view of the resistance right before the system enters the pure M phase. (b) Seebeck voltage measured across the middle segment of the VO$_2$ beam as a function of heater current. Inset: measured Seebeck voltage as a function of power dissipated in the heater. The relationship is consistently linear, as expected, for different samples and global temperatures.

(I) domains nucleating from the I (M) phase during the heating (cooling) process.[14] The resistance R_{total} is expected to consist of four parts

$$R_{total}(T_{global}) = x(T_{global})R_I(T_{global}) + [1 - x(T_{global})]R_M(T_{global}) + R_{contact} + R_{wall} \qquad (2)$$

where $x(T_{global})$ is the temperature-dependent length fraction of I phase in the segment. $R_I(T_{global})$ and $R_M(T_{global})$ are resistance of the pure I and M phases if they span the entire length, respectively. R_{wall} is the resistance from the M−I domain walls, and $R_{contact}$ is the electrode-VO$_2$ contact resistance and is expected to be zero in the four-probe measurements. As shown in the inset of Figure 3a, R_M is on the order of 75 Ω. The sudden drop of R_{total} (less than 10 Ω) right before the VO$_2$ becomes pure M phase must be caused by the sudden vanishing of the last I domain, therefore consisting of R_{wall} and $R_I - R_M$ of the last I domain. This implies that $R_{wall} < 10$ Ω. In any case, R_M, $R_{contact}$, and R_{wall} are much lower than R_I in the phase coexisting regime. Equation 2 can be approximated as $x(T_{global}) = R_{total}(T_{global})/R_I(T_{global})$, where $R_I(T_{global})$ is the extrapolation of the pure I-phase resistance to the phase-coexisting temperatures assuming the entire beam to be still in pure I phase. By measuring R_{total} over a wide range of T_{global}, we can determine $x(T_{global})$. This $x(T_{global})$ was used to analyze the measured Seebeck coefficient $S_{total}(T_{global})$ to extract the domain wall contribution.

Figure 3b shows the measured Seebeck voltage, $V_{hot} - V_{cold}$, from a VO$_2$ beam as a function of heater current. The measured $V_{hot} - V_{cold}$ is constantly positive, indicating n-type
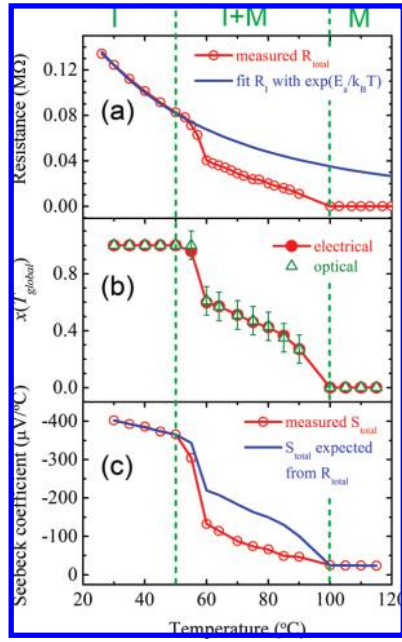
Figure 4. (a) Four-probe resistance of a VO₂ beam taken right after the Seebeck voltage measurement at each global temperature. Solid line is a fit of the resistance in pure I phase with standard equation and extrapolated to 120 °C. (b) Temperature-dependent I-phase length fraction, $x(T_{global})$, determined using electrical and optical methods, respectively. (c) Seebeck coefficient of a VO₂ beam measured as a function of temperature. Solid blue line is the Seebeck coefficient expected from the measured resistance in (a).

conduction in the VO₂, which is consistent with previous reports on bulk VO₂ crystals.[21,22] The conduction is n-type in the entire temperature range of the experiments, and no switch from n to p-type across the MIT was observed as reported by Kim et al.[23] $V_{hot} - V_{cold}$ depends on the heater current in a symmetric, quadratic shape, as shown by the parabolic fit in Figure 3b. The inset plots $V_{hot} - V_{cold}$ as a function of the Joule heating power dissipated in the heater. The relationship is consistently linear for different T_{global} and devices. The slope of the linear relationship gives the total Seebeck coefficient, S_{total}, after calibration of the temperature drop, $T_{hot} - T_{cold}$. To avoid overheating of the VO₂ beam by the local heater, we limited the power applied to the heater so that it was just high enough to generate sufficient temperature gradient ($T_{hot} - T_{cold} < 0.5$ °C) for a Seebeck parabola like Figure 3b to be recorded, but not too high as to affect R_{total}. For the maximum power dissipated in the heater, the change in R_{total} was less than 5%, which is negligible for the following thermopower analysis. To decouple the contributions of the domain walls from that of the M and I domains, T_{global} of the device was set by the global heater and the local heater current was scanned for measurement of S_{total} of the middle VO₂ segment; right after that, the local heater was turned off and the four-probe R_{total} of the same segment was measured. T_{global} was then tuned to the next value for another set of measurements. By doing so, we eliminated possible aging or hysteretic effects to ensure that S_{total} and R_{total} were measured while the VO₂ beam was in the same domain configuration.

As shown in Figure 4a, the VO₂ beam was initially in pure I phase until $T_{global} \sim 50$ °C; following that the beam entered the M−I phase coexistence regime (50 °C < T_{global} < 100 °C), and eventually became pure M phase at high temperatures (T_{global} > 100 °C). R_{total} in the pure I phase (namely, T_{global} < 50 °C) is R_I and was fitted using the standard equation for nondegenerately doped semiconductors, $R_I(T_{global}) = R_I^0 \cdot \exp(E_a/k_B T_{global})$. We determined E_a to be 0.2 eV, which compares to literature values of 0.3,[20] 0.13,[24] and 0.13−0.16 eV.[25] This fitted $R_I(T_{global})$ was extrapolated to higher temperatures, from which the fraction of the I phase in the middle segment was calculated using $x(T_{global}) = R_{total}(T_{global})/R_I(T_{global})$. Figure 4b shows $x(T_{global})$ determined by the measured $R_{total}(T_{global})$. For comparison, we also plot $x(T_{global})$ measured directly by optical imaging, which agrees very well with that obtained electrically. This agreement justifies the extrapolation of $R_I(T_{global})$ into the phase-coexisting temperature region.

In the pure I or M phase regimes, the Seebeck coefficient $S(T_{global})$ was obtained by dividing ($V_{hot} - V_{cold}$) with ($T_{hot} - T_{cold}$) according to eq 1. In the pure I phase regime, the expected temperature dependence of nondegenerately doped semiconductors is[26]

$$S_I(T) = \frac{k_B}{e}\left(\frac{5}{2} + r + \frac{|E_F|}{k_B T}\right) \quad (3)$$

where r is the power-law index for carrier scattering time in the Boltzmann transport theory, and $|E_F|$ is the Fermi energy measured from the bottom of the conduction band. Fitting eq 3 to the experimental data in the pure I phase regime, we obtained $|E_F| = 0.18$ eV, which well matches the activation energy of $E_a = 0.2$ eV, indicating that the Fermi level lies between the donor level and the conduction band minimum as expected. In the pure M phase, $S_M \approx$ const is expected for metals[27] at high temperatures. The measured S_I and S_M from all devices were in the range of $-300 \sim -400$ μV/°C and $-18 \sim -25$ μV/°C, respectively, which are consistent with reported values for bulk VO₂ of $-30 > S_I > -400$ μV/°C and $S_M = -21$ μV/°C.[22]

In the phase coexisting regime, as discussed before, the temperature gradient is still constant along the clamped VO₂ beam due to the much smaller thermal mass of the beam than that of the substrate. If one neglects the contribution from the M−I domain walls, the total Seebeck voltage is expected to be a sum of contributions from the M and I domains, $V_{hot} - V_{cold} = (-S_I)x(T_{hot} - T_{cold}) + (-S_M)(1 - x)(T_{hot} - T_{cold})$. It follows that the total Seebeck coefficient is expected to be

$$S_{total}(T_{global}) = x(T_{global})S_I(T_{global}) + [1 - x(T_{global})]S_M \quad (4)$$

where $S_I(T_{global})$ is extrapolated from the pure I phase regime. In eq 4, The measured $S_{total}(T_{global})$ is shown in Figure 4c together with the $S_{total}(T_{global})$ expected from eq 4. It can be seen that in the multiple M−I domain regime, the measured $S_{total}(T_{global})$ is significantly lower than the expected value,

differing by up to a factor of 2. Such a discrepancy was consistently observed from all the devices measured.

We briefly discuss the possible origin of this discrepancy. Recently Wei et al. reported that when a VO_2 beam is clamped at the two ends, self-developed uniaxial strain would drive it to move along the M−I phase boundary in the phase-coexisting regime; in this state the resistivity of I-phase VO_2 remains a constant as a function of temperature, no longer following $\exp(E_a/k_B T)$.[20] According to the authors' explanation, this is because the strain and temperature are coupled in this fixed-length beam. The tensile strain increases R_I in a manner to precisely cancel the reduction in R_I by temperature rise, so as to keep a constant free electron concentration along the M−I phase boundary. In our devices, however, the VO_2 beams were fully face-clamped to the substrate[14] instead of end−end clamped, therefore, the strain and temperature effects on R_I are expected not to coupled in the way as in ref 20. Moreover, using this mechanism to explain the discrepancy in Figure 4c would require that while the uniaxial tensile strain increases R_I to render R_I independent of T_{global} in the phase coexisting regime, it must not affect the T_{global} dependence of S_I. This requirement cannot be justified, as both S_I and R_I vary mainly through the change of free electron concentration.

It is known that the phase diagram of VO_2 is complicated when strain exists during the phase transition. For example, under strong compression perpendicular to (or tension along) the tetragonal c-axis, I-phase VO_2 passes through a second monoclinic phase (I_{M2}) before final transition into the M state.[28,29] The resistivity of I_{M2} is higher than that of the first monoclinic I phase (I_{M1}),[29] which might affect the accuracy of our electrically determined $x(T_{global})$ where extrapolation of purely I_{M1} phase was used. As shown in Figure 4b, however, the electrically determined $x(T_{global})$ by assuming no I_{M2} phase is nearly identical to that measured directly using optical microscopy. This indicates that there was no transition from I_{M1} to I_{M2} phase in the temperature region of interest in our devices. The absence of I_{M2} phase in the system is understandable, because the transition from I_{M1} to I_{M2} occurs only at certain conditions with strong tensile strain. The clamped VO_2 beam might have been already in I_{M2} phase at room temperature due to large initial axial tension[29] and thus directly enters M phase when heated up; or the system might be initially in highly compressive axial strain, so that it is in compressed I_{M1} and does not pass the I_{M2} phase at all during the transition to M phase. One could significantly reduce the expected $S_{total}(T_{global})$ toward the measured $S_{total}(T_{global})$ by including I_{M2} domains only under the assumptions that (A) the resistivity of I_{M2} is equal to that of I_{M1}, yet (B) its Seebeck coefficient is much lower than that of I_{M1}. However, this requirement is difficult to justify, as in nondegenerately doped semiconductors, resistivity, and Seebeck coefficient are linked to each other through free carrier concentration. More detailed discussions are given in Supporting Information.

We therefore believe that the discrepancy in Figure 4c is caused by the neglected domain wall contribution (S_{wall}) to S_{total} in eq 4. If this contribution is added, S_{wall} must have the opposite sign and comparable magnitude as S_I. This effect is unexpected in the framework of mere thermionic emission across a Schottky junction.[6] It is possible that complications of the phase coexistence near the domain wall cause a deviation of the Seebeck effect from a normal behavior in the pure states. It has been reported that at the M−I phase boundary, the MIT is not simply an electronic transition from a Mott insulator to a normal metal. For example, Kim et al. reported a sudden increase of hole concentration in the I state in close vicinity of the MIT.[23,30] Qazilbash et al. reported that very close to the M−I phase boundary, the M state behaves differently from the M phase far from the boundary with a diverging effective electron mass.[31] All these nonlinear effects are possibly responsible for the discrepancy shown in Figure 4c, because an explanation of it would require the I or M phase near the phase boundary to behave differently from a simple extrapolation of the pure phase. Further theoretical as well as experimental investigations are needed for elucidation of this effect.

In summary, we have measured the Seebeck effect of single-crystal VO_2 microbeams across their metal−insulator phase transition. In the temperature range where the metal and insulator phases coexist with one-dimensionally aligned M−I domain arrays separated by domain walls, the measured Seebeck coefficient is significantly lower than a linear combination of the contributions from the I and M domains. The discrepancy is discussed in the context of the contribution of the metal−insulator domain walls and possible deviation from linear extrapolation of the behavior of pure M and I phases.

Supporting Information Available: This material is available free of charge via the Internet at http://pubs.acs.org.

References

(1) Majumdar, A. *Science* **2004**, *303*, 777.
(2) Boukai, A. I.; Bunimovich, T.; Tahir-Kheli, J.; Yu, J. K.; Goddard, W. A.; Heath, J. R. *Nature* **2008**, *451*, 168.
(3) Hochbaum, A. I.; Chen, R.; Delgado, R. D.; Liang, W.; Garnett, E. C.; Najarian, M.; Majumdar, A.; Yang, P. D. *Nature* **2008**, *451*, 163.
(4) Heremans, J. P.; Jovovic, V.; Toberer, E. S.; Saramat, A.; Kurosaki, K.; Charoenphakdee, A.; Yamanaka, S.; Snyder, G. J. *Science* **2008**, *321*, 554.
(5) Mahan, G. D.; Sofo, J. O. *Proc. Natl. Acad. Sci. U.S.A.* **1996**, *93*, 7436.
(6) Mahan, G. D.; Sofo, J. O.; Bartkowiak, M. *J. Appl. Phys.* **1998**, *83*, 4683.
(7) Vashaee, D.; Shakouri, A. *Phys. Rev. Lett.* **2004**, *92*, 106103.
(8) Mahan, G. D.; Woods, L. M. *Phys. Rev. Lett.* **1998**, *80*, 4016.
(9) Zeng, G.; Zide, J. M. O.; Kim, W.; Bowers, J. E.; Gossard, A. C.; Bian, Z.; Zhang, Y.; Shakouri, A.; Singer, S. L.; Majumdar, A. *J. Appl. Phys.* **2007**, *101*, 034502.
(10) Duarte, N. B.; Mahan, G. D.; Tadigadapa, S. *Nano Lett.* **2009**, *9*, 617.
(11) Eyert, V. *Ann. Phys.-Berlin* **2002**, *11* (9), 650.

(12) Rakotoniaina, J. C.; Mokranitamellin, R.; Gavarri, J. R.; Vacquier, G.; Casalot, A.; Calvarin, G. *J. Solid State Chem.* **1993**, *103* (1), 81.

(13) Marezio, M.; McWhan, B.; Dernier, P. D.; Remeika, J. P. *Phys. Rev. B* **1972**, *5* (7), 2541.

(14) Wu, J.; Gu, Q.; Guiton, B. S.; de Leon, N.; Lian, O.; Park, H. *Nano Lett.* **2006**, *6*, 2313.

(15) Fisher, B. *J. Phys. C: Solid State Phys.* **1976**, *9* (7), 1201.

(16) Gu, Q.; Falk, A.; Wu, J.; Ouyang, L.; Park, H. *Nano Lett.* **2007**, *7*, 363.

(17) Guiton, B. S.; Gu, Q.; Prieto, A. L.; Gudiksen, M. S.; Park, H. *J. Am. Chem. Soc.* **2005**, *127*, 498.

(18) Cao, J.; Ertekin, E.; Srinivasan, V.; Fan, W.; Huang, S.; Zheng, H.; Yim, J. W. L.; Khanal, D. R.; Ogletree, D. F.; Grossman, J. C.; Wu, J. *Nat. Nanotechnol.*, in press.

(19) Liang, W.; Hochbaum, A. I.; Fardy, M.; Rabin, O.; Zhang, M.; Yang, P. D. *Nano Lett.* **2009**, *9*, 1689.

(20) Wei, J.; Wang, Z.; Chen, W.; Cobden, D. H. *Nat. Nanotechnol.* **2009**, *4*, 420.

(21) Fisher, B. *J. Phys. C: Solid State Phys.* **1975**, *8* (13), 2072.

(22) Berglund, C. N.; Guggenheim, H. J. *Phys. Rev.* **1969**, *185*, 1022.

(23) Kim, H. T.; Chae, B. G.; Youn, D. H.; Maeng, S. L.; Kim, G.; Kang, K. Y.; Lim, Y. S. *New J. Phys.* **2004**, *6*, 52.

(24) Wu, X.; Tao, Y.; Dong, L.; Wang, Z.; Hu, Z. *Mater. Res. Bull.* **2005**, *40* (2), 315.

(25) Guinneton, F.; Sauques, L.; Valmalette, J. C.; Cros, F.; Gavarri, J. R. *J. Phys. Chem. Solids* **2001**, *62*, 1229.

(26) Cai, J.; Mahan, G. D. *Phys. Rev. B* **2006**, *74*, 075201.

(27) MacDonald, D. K. C. *Thermoelectricity: an introduction to the principles*; John Wiley & Sons, Inc.: New York, 1962.

(28) Pouget, J. P.; Launois, H.; D'Haenens, J. P.; Merenda, P.; Rice, T. M. *Phys. Rev. Lett.* **1975**, *35*, 873.

(29) Cao, J.; Fan, W.; Ogletree, D. F.; Wu, J. Unpublished work, 2009.

(30) Kim, H. T.; Lee, Y. W.; Kim, B. J.; Chae, B. G.; Yun, S. J.; Kang, K. Y.; Han, K. J.; Yee, K. J.; Lim, Y. S. *Phys. Rev. Lett.* **2006**, *97*, 266401.

(31) Qazilbash, M. M.; Brehm, M.; Chae, B. G.; Ho, P. C.; Andreev, G. O.; Kim, B. J.; Yun, S. J.; Balatsky, A. V.; Maple, M. B.; Keilmann, F.; Kim, H. T.; Basov, D. N. *Science* **2007**, *318*, 1750.

NL902167B

Supplementary information for "Thermoelectric Effect across the Metal-Insulator Domain Walls in VO$_2$ Microbeams"

J. Cao,[1, 2, †] W. Fan,[1, 3, †] H. Zheng,[2,4] and J. Wu [1, 2,*]

[1]Department of Materials Science and Engineering, University of California, Berkeley, Berkeley, CA 94720, USA

[2]Materials Sciences Division, Lawrence Berkeley National Laboratory, Berkeley, CA 94720, USA

[3]Department of Thermal Science and Energy Engineering, University of Science and Technology of China, Hefei, China

[4]National Center for Electron Microscopy, Lawrence Berkeley National Laboratory, Berkeley, CA 94720, USA

[†] These authors contributed equally to this work.

*To whom correspondence should be addressed. Email: wuj@berkeley.edu

1. Expected thermoelectric effect over M-I junctions in VO$_2$

For a homogeneous semiconductor (e.g., a pure I-phase VO$_2$ which is a n-type semiconductor) with length L_I and electrical conductivity σ, when it is simultaneously electrically (ΔV) and thermally (ΔT) biased, a drift current ($\sigma \cdot \Delta V / L_I$) will carry a net heat flowing along the electron flow direction. The total heat flux is described by the well known Peltier effect [1],

$$J_Q = \Pi \cdot \sigma \cdot \Delta V / L_I - K \cdot \Delta T / L_I , \qquad (S1)$$

where Π is the Peltier coefficient, K is the thermal conductivity associated with diffusion current. The total electrical current is [1]

$$J_e = \sigma \cdot \Delta V / L_I + \sigma \cdot S \cdot \Delta T / L_I . \qquad (S2)$$

where S is the Seebeck coefficient. Under open circuit condition, $J_e = 0$, we can have the Seebeck coefficient measured,

$$S = -\Delta V / \Delta T . \qquad (S3)$$

The Peltier and Seebeck coefficients are related to each other by the Kelvin-Thomson relationship [1, 2],

$$\Pi = S \cdot T . \qquad (S4)$$

Therefore, an effectively enhanced Peltier effect in a system is expected to cause an enhanced Seebeck effect, and hence a higher Seebeck e.m.f. (ΔV) measured under open-circuit condition.

The situation is complicated when junction exists in a heterogeneous system. Figure S1 Shows the schematic view of Peltier effect across the two metal-semiconductor junctions in a VO$_2$ beam where an I domain is sandwiched between two M domains [3-5]. Compared to the pure I phase VO$_2$, the system has two junctions whose Schottky barriers act as the electron filter, causing additional junction Peltier effect: When it is electrically and/or thermally biased so that an electric field is established in the system, directional symmetry is broken and a drift current will flow. Hot

electrons (i.e., electrons with energy above the Fermi level) escape across the barrier from the M-phase at the reversely biased junction (right-hand-side junction), effectively cooling this junction [6]. At the forward biased junction (left-hand-side junction), electrons are injected from I to M phase, becoming hot electrons in the M phase and effectively heating the junction [6]. Between these two junctions, therefore, additional heat flux is carried along by the conductive electrons and flows in the direction as shown in Fig.S1. This heat flow is caused by the M-I junctions, and effectively adds onto the original Peltier heat flow of a pure I-phase VO_2 in the absence of the junction (Eq.S1). This is the basic principle behind the proposed thermionic cooling devices [7, 8].

Here the hot-electron barrier at each junctions is the Schottky junction depletion region (width w)

Fig. S1 Schematic view of Peltier effect across the M-I domain walls in VO_2. When electrically biased, hot electrons are filtered across the barrier at one junction and driven toward the other one, effectively cooling the reversely biased junction and heating the forward biased one. L_I is the I-domain length and w is the Schottky junction depletion width.

inside the I phase, and not the entire I domain (length L_I). w is estimated to be on the order of 15 nm (assuming barrier height 0.3 eV and doping $\sim 10^{19}\,cm^{-3}$), which is smaller than typical mean free path of electrons ($\lambda \sim 100$ nm) [7], thus allowing ballistic transport across the barrier. The value of L_I, on the other hand, does not play a role in this effect, and therefore can be much larger ($\sim \mu$m) than λ.

At high drift current, both this Peltier effect and Joule heating are sufficiently strong, so that the Peltier cooling in the reversely biased junction converts the neighboring M phase into I phase, and the Peltier heating in the forward biased junction converts the neighboring I phase into M phase. As a result, the entire I domain in Fig. S1 starts to drift against the electron flow direction (i.e., along the current direction). Such a domain growth and/or drifting in VO_2 has been directly observed optically by Raikhtsaum et al. [4] and Fisher et al. [3] in the 1970s, and recently electrically by Gu et al. through coupling to an external R-C circuit [5].

When Fig.S1 is thermally biased and open-circuit, the net current is zero due to the cancellation between drift current and diffusion current in Eq.S2. Both currents are weak so as unable to cause domain wall drifting. However, the junction-enhanced Peltier effect leads to an enhanced Seebeck effect through Eq.S4, and therefore an increase in Seebeck voltage is expected as compared to a junction-free, pure I-phase specimen (after domain length normalization).

2. Effect of possible existence of I_{M2} domains on the data analysis

It is known that the phase diagram of VO_2 is complicated when uniaxial strain exists [9]. Namely, in addition to the regular I_{M1} phase, another monoclinic, insulating phase (I_{M2}) might show up if the specimen is tensile strained along the tetragonal c-axis direction (or compression perpendicular to c-direction). I_{M2} phase is believed to have a resistivity higher than that of I_{M1}
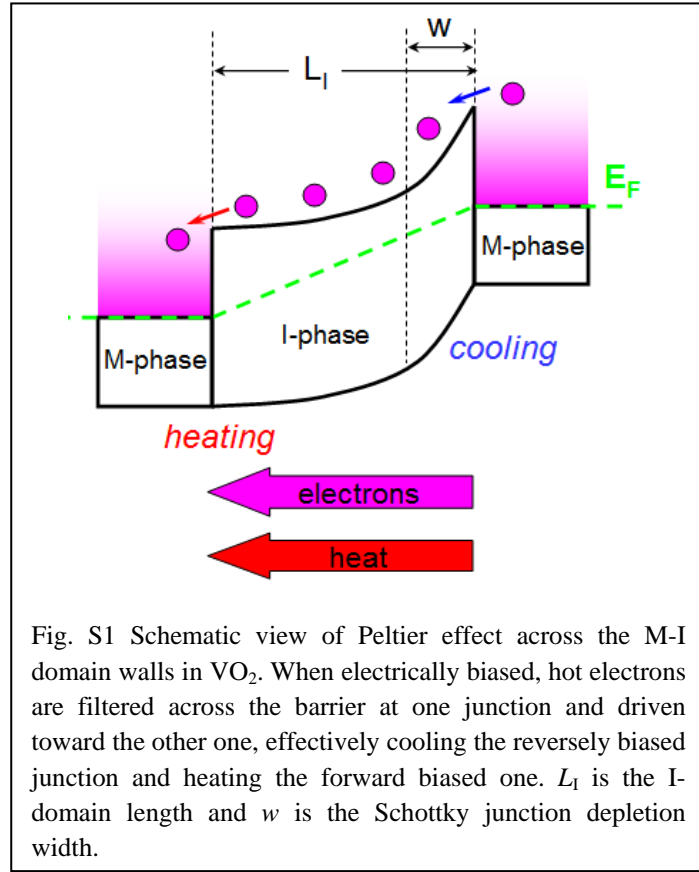
phase [10, 11], and optically identical to I_{M1} phase. Emergence of I_{M2} domains along the VO_2 beam in the multi-domain temperature range might cause an overestimate of $x(T_{global})$, and yield a higher expected $S_{total}(T_{global})$. However, such possibility is ruled out by the fact that $x(T_{global})$ measured optically is nearly identical to that deduced electrically (main text Fig. 4(b)) under the assumption of having no I_{M2} phases. The absence of I_{M2} phase in the system is understandable, because the transition from I_{M1}-I_{M2} occurs only at strong tensile strain conditions [9]. The VO_2 beam might have been already in a pure I_{M2} phase at room temperature due to its large initial axial tensile stress and thus directly enters M phase when heated up, or the system might be initially in highly compressive axial strain, so that it is in compressed I_{M1} phase and would not pass the I_{M2} phase at all during the phase transition to M phase.

Here we expand our discussion about the effect of possible I_{M2} domains on the thermoelectric measurements, and further demonstrate that the measured low Seebeck coefficient is unlikely to be caused by the emergence of I_{M2} domains. Assuming that domains of all three phases (I_{M1}, I_{M2}, and M) coexist at the phase-coexisting temperatures at their respective fractions, and there is no junction contribution, it follows that the total resistance and Seebeck coefficient are expected to be

$$R_{total} = x_{I_{M1}} \cdot R_{I_{M1}} + x_{I_{M2}} \cdot R_{I_{M2}} + \left[1 - x_{I_{M1}} - x_{I_{M2}} \right] \cdot R_M , \tag{S5}$$

$$S_{total} = x_{I_{M1}} \cdot S_{I_{M1}} + x_{I_{M2}} \cdot S_{I_{M2}} + \left[1 - x_{I_{M1}} - x_{I_{M2}} \right] \cdot S_M . \tag{S6}$$
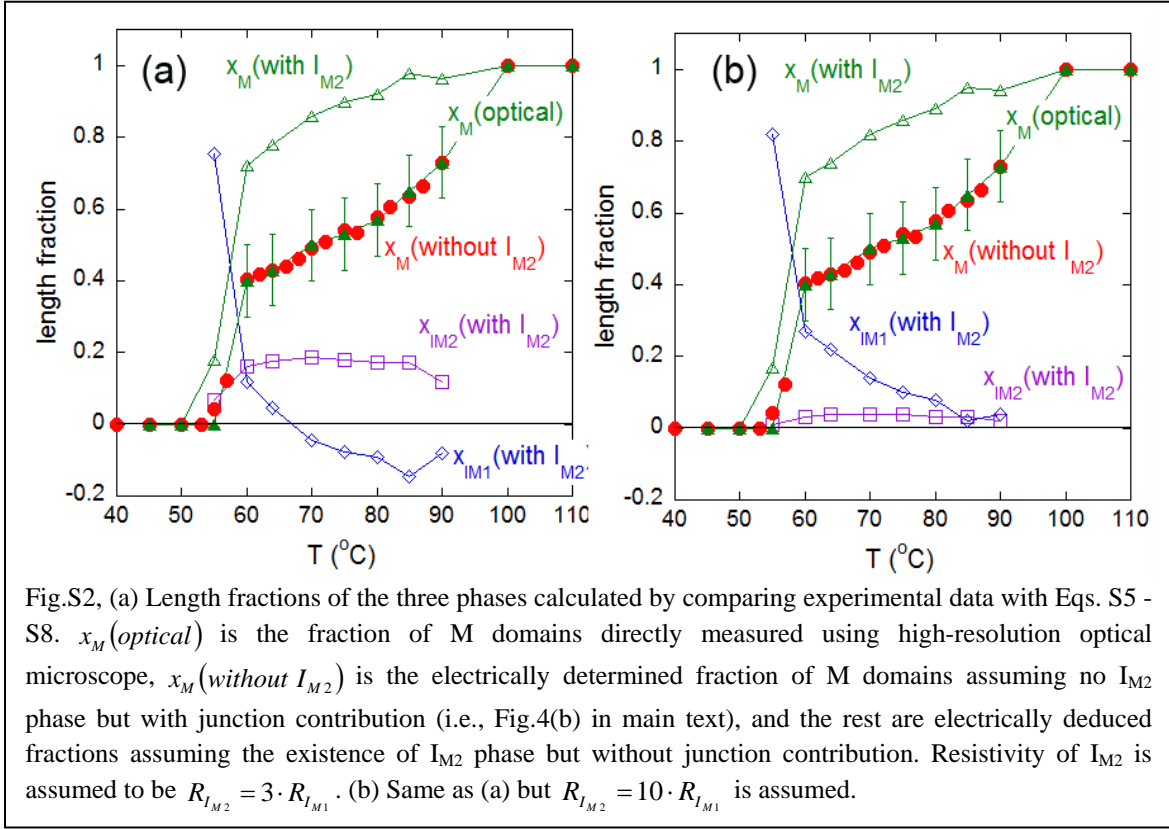
The temperature dependence of S for non-degenerately doped semiconductors is [1, 2]

$$S_I(T) = \frac{k_B}{e} \left(\frac{5}{2} + r - \ln \frac{n_I}{N_C} \right), \tag{S7}$$

and pure-phase resistance (proportional to resistivity) is

$$R_I \propto n_I \cdot \mu , \tag{S8}$$

where n_I is the free electron concentration and $N_C = 2\left(m^* k_B T / 2\pi\hbar^2 \right)^{3/2}$ is the effective density of states. We assume equal carrier mobility (μ) and N_C for I_{M1} and I_{M2} phases, and $R_{I_{M2}} = 3 \cdot R_{I_{M1}}$ according to Wei et al.[11] (therefore we attribute the higher resistivity in I_{M2} phase to its lower n_I). Equations S7 and S8 link the difference in R_I between I_{M1} and I_{M2} phases to their difference in S_I. We then calculate $x_{I_{M1}}$, $x_{I_{M2}}$ and $x_M = 1 - x_{I_{M1}} - x_{I_{M2}}$ by forcing Eqs.(S5) and (S6) to be equal to experimentally measured R_{total} and S_{total}, respectively, at each temperature. We plot the obtained length fractions in Fig.S2(a). It is clear that the inclusion of I_{M2} phase causes non-physical, negative values of $x_{I_{M1}}$. Next, assuming $R_{I_{M2}} = 10 \cdot R_{I_{M1}}$ instead, we reach values as shown in Fig.S2(b). In both Figs.S2(a) and (b), the evident disagreement between deduced x_M and optically measured $x_M(optical)$ is much larger than the experimental error (≈ 0.1) of $x_M(optical)$. Without taking into account junction contribution, no value of $R_{I_{M2}}/R_{I_{M1}}$ ratio allows a simultaneous fit to the measured R_{total} and S_{total}. These analyses demonstrate that the unusually low Seebeck coefficient in the M-I coexisting regime cannot be explained by possible existence of I_{M2} domains in the system.

3

Fig.S2, (a) Length fractions of the three phases calculated by comparing experimental data with Eqs. S5 - S8. $x_M(optical)$ is the fraction of M domains directly measured using high-resolution optical microscope, $x_M(without\ I_{M2})$ is the electrically determined fraction of M domains assuming no I_{M2} phase but with junction contribution (i.e., Fig.4(b) in main text), and the rest are electrically deduced fractions assuming the existence of I_{M2} phase but without junction contribution. Resistivity of I_{M2} is assumed to be $R_{I_{M2}} = 3 \cdot R_{I_{M1}}$. (b) Same as (a) but $R_{I_{M2}} = 10 \cdot R_{I_{M1}}$ is assumed.

References

1.   Cai, J.; Mahan, G. D. *Phys. Rev. B* **2006,** 74, 075201.
2.   MacDonald, D. K. C., *Thermoelectricity: an introduction to the principles*. John Wiley & Sons, Inc.: New York, 1962.
3.   Fisher, B. *J. Phys. C Solid State Phys.* **1976,** 9, (7), 1201.
4.   Raikhtsaum, G. A.; Slyshek, N. V.; Chudnovskii, F. A. *Sov. Phys. Semicon.* **1973,** 6, 1906.
5.   Gu, Q.; Falk, A.; Wu, J.; Ouyang, L.; Park, H. *Nano Lett.* **2007,** 7, 363.
6.   West, A. R., *Solid State Chemistry and Its Applications*. John Wiley & Sons Ltd.: 1984.
7.   Mahan, G. D.; Sofo, J. O.; Bartkowiak, M. *J. Appl. Phys.* **1998,** 83, 4683.
8.   Mahan, G. D.; Woods, L. M. *Phys. Rev. Lett.* **1998,** 80, 4016.
9.   Pouget, J. P.; Launois, H.; D'Haenens, J. P.; Merenda, P.; Rice, T. M. *Phys. Rev. Lett.* **1975,** 35, 873.
10.   Zylbersztejn, A.; Mott, N. F. *Phys. Rev. B* **1975,** 11, (11), 4383.
11.   Wei, J.; Wang, Z.; Chen, W.; Cobden, D. H. *unpublished* **2009**.